

Hole-Doping Effect on Superconductivity in Compressed CeH₉ at High Pressure

Chongze Wang¹, Shuyuan Liu¹, Hyunsoo Jeon¹, Seho Yi¹, Yunkyu Bang^{2,3}, and Jun-Hyung Cho^{1,3*}

¹ Department of Physics, Research Institute for Natural Science,
and Institute for High Pressure at Hanyang University, Hanyang University,
222 Wangsimni-ro, Seongdong-Ku, Seoul 04763, Republic of Korea

² Department of Physics, Pohang University of Science and Technology, Pohang 37673, Republic of Korea

³ Asia Pacific Center for Theoretical Physics (APCTP),
Pohang-si, Gyeongsangbuk-do 37673, Republic of Korea

(Dated: December 23, 2024)

The experimental realization of high-temperature superconductivity in compressed hydrides H₃S and LaH₁₀ at high pressures over 150 GPa has aroused great interest in reducing the stabilization pressure of superconducting hydrides. For cerium hydride CeH₉ recently synthesized at 80–100 GPa, our first-principles calculations reveal that the strongly hybridized electronic states of Ce 4*f* and H 1*s* orbitals around the Fermi energy E_F produce the topologically nontrivial Dirac nodal lines protected by crystalline symmetries in the presence of spin-orbit coupling. By hole doping, E_F shifts down toward the topology-associated van Hove singularity to significantly increase the density of states, which in turn raises a superconducting transition temperature T_c from 74 K up to 136 K at 100 GPa. The hole-doping concentrations can be controlled by the incorporation of Ce³⁺ ions with varying their percentages, which can be well electronically miscible with Ce atoms in the CeH₉ matrix because both Ce³⁺ and Ce behave similarly as cations. Therefore, the interplay of symmetry, band topology, and hole doping contributes to enhance T_c in compressed CeH₉. This mechanism to enhance T_c can also be applicable to another superconducting rare earth hydride LaH₁₀.

Doping in condensed matters is a well-established means of manipulating their electronic structures, which may lead to the emergence of various quantum phases with exotic physical properties [1–7]. For example, in the unconventional high-temperature superconductors such as cuprates [8] and pnictides [9, 10], doping by holes or electrons has been demonstrated not only to induce complex quantum phase transitions including magnetism, pseudogap, charge density wave, superconductivity (SC), and Fermi liquid phases, but also to vary T_c in their superconducting phases [4–7]. Due to the emergence of such many electronic states in unconventional high- T_c superconductors, identifying the mechanism responsible for the doping-induced changes of T_c has been elusive. By contrast, doping effect in conventional Bardeen-Cooper-Schrieffer (BCS) [11] superconductors has been relatively well understood in terms of the influence of electron-phonon coupling (EPC), and therefore various dopants can be employed to tune T_c . It is thus very interesting and challenging to investigate the effect of doping on the EPC-driven SC of recently discovered hydrides at high pressures.

During the past six years, compressed hydrides under megabar pressures have attracted much attention because of their unprecedented records of T_c . Motivated by the theoretical predictions of SC in a number of hydrides [12–21], experiments have confirmed that sulfur hydride H₃S and lanthanum hydride LaH₁₀ exhibit T_c around 203 K at \sim 155 GPa [22] and 250–260 K at \sim 170 GPa [23, 24], respectively. More recently, carbonaceous sulfur hydride was experimentally realized to reach a room-temperature SC with a T_c of 288 K at \sim 267 GPa [25]. Despite such an achievement of room-temperature SC, it is highly demanding to discover high- T_c superconducting hydrides synthesized at moderate pressures below \sim 100 GPa, which can be normally achievable with the diamond anvil cell [26, 27]. Near simultaneously, two ex-

perimental groups [28, 29] reported the successful synthesis of cerium hydride CeH₉ at 80–100 GPa. The subsequent density-functional theory (DFT) calculation of CeH₉ revealed that the delocalized nature of Ce 4*f* electrons is an essential ingredient in the high chemical precompression of clathrate H cage around Ce atom [see Fig. 1(a)]. It is noticeable that, even though the synthesis of CeH₉ was made at lower pressures below \sim 100 GPa, its theoretically predicted T_c value was around 75 K [18, 29], much lower than those of H₃S and LaH₁₀ [22–24]. Therefore, the main bottleneck for the research of high- T_c superconducting hydrides has been associated with difficulties both raising T_c and lowering the pressure of stability. In order to alleviate this bottleneck in CeH₉, we here investigate the effect of hole doping on SC, which leads to a significant increase in T_c .

For high-pressure rare earth hydrides with clathrate H-cage structures, the electronic states tend to have a strong hybridization between rare earth-4*f* and H-1*s* orbitals near E_F [19, 28–32]. This electronic characteristic of rare earth hydrides having high-symmetry structures could be favorable for hosting topological states through band inversions, identified in recent studies of topological materials [30]. As compelling examples, topologically nontrivial Dirac-nodal-line (DNL) states are jointly protected by the space inversion symmetry P and time-reversal symmetry T supplemented by additional crystalline symmetry [33–36]. However, exploration of the cooperative interplay of crystal symmetry and band topology has so far been overlooked in high-pressure superconducting hydrides. These new ingredients of symmetry and topology together with hole doping will provide a promising playground to enhance T_c in high-pressure superconducting hydrides, as will be demonstrated later.

In this Letter, using first-principles calculations, we discover that CeH₉ possessing a hexagonal-close-packed (hcp)

structure has symmetry-enforced DNL states. It is revealed that the two-dimensional (2D) nodal surface guaranteed by the nonsymmorphic crystal symmetry S_{2z} (equivalent to the combination of twofold rotation symmetry C_{2z} about the z axis and a half translation along the z direction) is converted to one-dimensional (1D) DNLs in the presence of spin-orbit coupling (SOC) [37]. Moreover, these Dirac fermion states composed of strongly hybridized Ce $4f$ and H $1s$ orbitals produce a van Hove singularity (vHs) around -1.6 eV below E_F . Consequently, hole doping shifts E_F toward the vHs, which in turn increases EPC and therefore raises T_c from 74 K (without hole doping) up to 136 K at 100 GPa. Considering that Ce atoms in the CeH₉ matrix behave as cations, Ce³⁺ ions is expected to be well electronically miscible with Ce atoms and their incorporation percentages can control hole-doping concentrations. Our findings provide a new avenue for using hole doping to enhance T_c in recently synthesized rare earth hydrides CeH₉ as well as LaH₁₀.

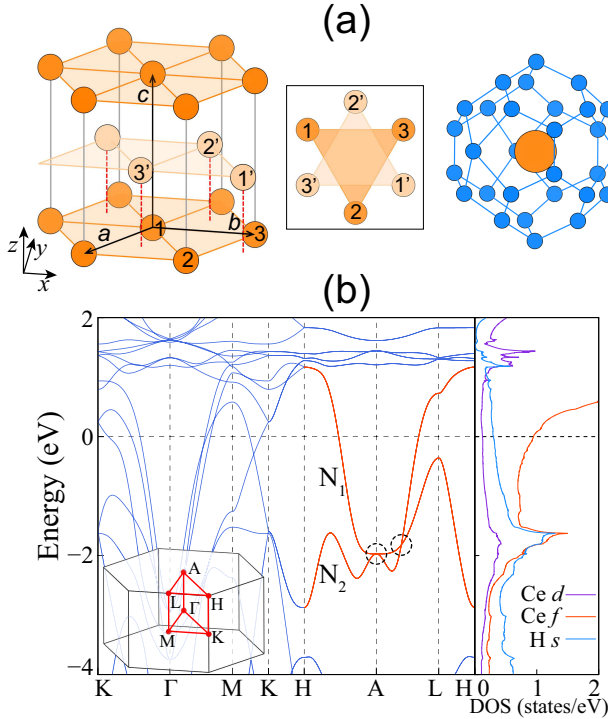


FIG. 1. (a) Optimized hcp structure of Ce atoms in CeH₉. The inset shows the top view of Ce atoms, and the isolated H₂₉ cage surrounding a Ce atom is also included. The calculated band structure of CeH₉ together with the PDOS for Ce $4f$, Ce $5d$, and H $1s$ orbitals is given in (b). N_1 and N_2 represent the fourfold degenerate bands along the high-symmetry H - A - L - H paths, and the energy zero is E_F . The Brillouin zone of hcp structure is also included in (b).

We first present the electronic band structure of hcp CeH₉, obtained using first-principles DFT calculations [38]. In most of the calculations hereafter, we fix a pressure of 100 GPa at which the hcp phase with the lattice parameters $a = b = 3.698$ Å and $c = 5.596$ Å [see Fig. 1(a)] is thermodynamically stable [see Fig. S1(a) in the Supplemental Material [47]]. It

is noted that at 70 GPa, the hcp phase becomes dynamically unstable with the presence of imaginary phonon modes [see Fig. S1(b)]. Figure 1(b) shows the calculated band structure and partial density of states (PDOS) of CeH₉. We find that the Ce $4f$ and H $1s$ orbitals are more dominant components in the electronic states around E_F , compared to other orbitals (see Fig. S2 of the Supplemental Material [47]). Interestingly, the PDOS for Ce $4f$ and H $1s$ orbitals exhibits a sharp peak around -1.6 eV below E_F [see Fig. 1(b)], indicating a strong hybridization of the two orbitals. The existence of such a vHs having large DOS leads to an increase of T_c via hole doping, as discussed below.

Figure 1(b) shows the DFT band structure computed without including SOC. The presence of P and T symmetries ensures Kramer's double degeneracy in the whole Brillouin zone (BZ). We find that there are fourfold degenerate bands N_1 and N_2 along the high-symmetry H - A - L - H paths, formed by touching of two bands. It is noted that N_1 and N_2 touch each other at A and between A and L [marked by dashed circles in Fig. 1(c)], thereby giving rise to eightfold accidental degeneracies. Using the tight-binding Hamiltonian with a basis of maximally localized Wannier functions [48, 49], we reveal the existence of 2D nodal surfaces NS_1 and NS_2 throughout the $k_z = \pi/c$ plane, as shown in Fig. 2(a). Here, each nodal surface is formed by a touching of two doubly-degenerate bands at the boundary of BZ. Since the crystalline symmetry of hcp CeH₉ belongs to the space group $P6_3/mmc$ (No. 194) with the point group D_{6h} , the fourfold degeneracy of NS_1 and NS_2 is respected by the combined symmetry $S_{2z}P$, whose eigenvalues are ± 1 because of $(S_{2z}P)^2 = 1$ (see symmetry analysis in the Supplemental Material [47]). The inclusion of SOC lifts the degeneracy of N_1 and N_2 along the H - A - L - H paths except A - L (see Fig. S3 in the Supplemental Material [47]), where the SOC-induced gap opening is less than ~ 0.1 eV. It is noted that the nodal surfaces NS_1 and NS_2 are converted into 1D nodal lines along the high-symmetry paths $k_x = 0$ and $k_x = \pm\sqrt{3}k_y$ as well as with circular patterns around the A point [see Fig. 2(b)]. These DNLs showing C_{3z} rotation symmetry are protected by additional mirror symmetry (see symmetry analysis in the Supplemental Material [47]). For example, $M_x : (x, y, z) \rightarrow (-x, y, z)$ anticommuting with $S_{2z}P$ allows the existence of the fourfold degenerate nodal line at $k_x = 0$ and $k_z = \pi/c$. The topological characterizations of these DNLs are demonstrated by calculating the topological index [36], defined as $\zeta_1 = \frac{1}{\pi} \oint_c dk \cdot A(k)$, along a closed loop encircling any of the DNLs. Here, $A(k) = -i \langle u_k | \partial_k | u_k \rangle$ is the Berry connection of the related Bloch bands. We obtain $\zeta_1 = \pm 1$ for the DNLs, indicating that they are stable against $S_{2z}P$ and M symmetries conserving perturbations.

As shown in Figs. 1(b) and 2(a), the position of vHs arising from the saddle points of energy dispersion is located near the band crossings of N_1 (NS_1) and N_2 (NS_2). It is thus likely that crystalline symmetries producing the nontrivial band topology of CeH₉ are correlated with the existence of vHs. In other words, the present vHs is rendered emergent by the crossings of the two fourfold degenerate topological states below E_F

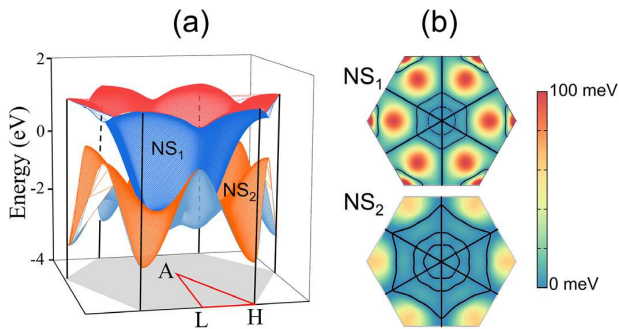


FIG. 2. (a) Energy of 2D nodal surfaces NS_1 and NS_2 throughout the $k_z = \pi/c$ plane, obtained without including SOC and (b) 1D nodal lines converted from NS_1 and NS_2 with including SOC. In (b), the SOC-induced gap is represented using the color scale in the range between 0 and 100 meV.

and yield a power law divergence in the DOS [50], which in turn enhances T_c via hole doping, as discussed below.

To estimate T_c of CeH_9 at 100 GPa, we calculate the phonon spectrum, the projected phonon DOS onto Ce and H atoms, the Eliashberg function $\alpha^2F(\omega)$, and the integrated EPC constant $\lambda(\omega)$ as a function of phonon frequency. Figure 3(a) shows that the phonon spectrum is divided into two regimes: i.e., one is the low-frequency regime arising from the vibrations of Ce atoms and the other is the high-frequency regime driven by H atoms. Therefore, we find that the acoustic phonon modes of Ce atoms contribute to $\sim 19\%$ of the total EPC constant $\lambda = \lambda(\infty)$, whereas the optical phonon modes of H atoms contribute to $\sim 81\%$ of λ . Specifically, the H-derived low-frequency optical modes close to the Ce-derived acoustic modes show larger EPC strength, as represented by circles on the phonon dispersion in Fig. 3(a). Based on these results, we can say that the optical vibrations of H atoms are strongly coupled to the hybridized electronic states of Ce $4f$ and H $1s$ orbitals around E_F , giving rise to $\lambda = 1.04$. By numerically solving the isotropic Migdal-Eliashberg equations [51–53], we calculate the superconducting gap versus temperature with varying Coulomb pseudopotential parameter μ^* [18, 29], and estimate $T_c \approx 84$ and 74 K with $\mu^* = 0.1$ and 0.13 , respectively [see Fig. 3(b)]. Here, the predicted T_c values in CeH_9 are much reduced, compared to the observed T_c values of ~ 200 and ~ 260 K for H_3S [22] and LaH_{10} [23, 24], respectively. The lower T_c in CeH_9 is partly associated with fewer EPC channels compared to the cases of H_3S and LaH_{10} , because CeH_9 has relatively smaller DOS at E_F than H_3S and LaH_{10} (see Fig. S4 in the Supplemental Material [47]).

Since a vHs in the electronic DOS is located below E_F [see Fig. 1(b)], hole doping is expected to induce a shift of E_F toward the vHs. The calculated band structure at a hole doping of $n_h = 1.0e$ per Ce atom shows that E_F approaches the vHs, thereby giving rise to an increase of DOS around E_F (see Fig. S5 in the Supplemental Material [47]). In order to examine how the hole doping influences SC, we use the isotropic Migdal-Eliashberg formalism [51–53] to estimate the varia-

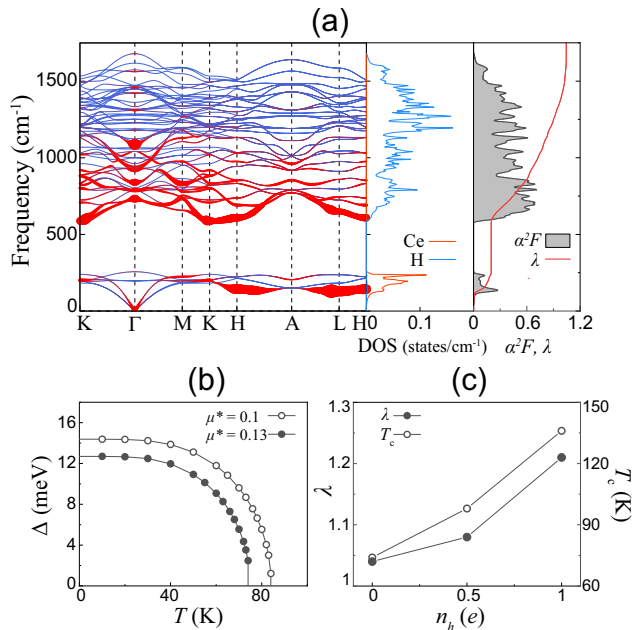


FIG. 3. (a) Calculated phonon spectrum, phonon DOS projected onto Ce and H atoms, Eliashberg function $\alpha^2F(\omega)$, and integrated EPC constant $\lambda(\omega)$ of CeH_9 , (b) superconducting energy gap Δ as a function of temperature with $\mu^* = 0.1$ and 0.13 , and (c) λ and T_c as a function of n_h .

tions of λ and T_c as a function of n_h . As shown in Fig. 3(c), λ is enhanced from 1.04 (without hole doping) to 1.08 and 1.21 at $n_h = 0.5$ and $1.0e$, respectively, which in turn increases T_c up to 136 K at $n_h = 1.0e$. It is thus likely that the increased DOS around E_F via hole doping increases the EPC channels, resulting in an increase of T_c . We note that hole doping with $n_h < 1.2e$ preserves structural stability without imaginary phonon frequencies (see Fig. S6 in the Supplemental Material [47]).

Although ordinary hole doping is achieved by the introduction of electron acceptor dopants in the host matrix, we here propose the hole doping of CeH_9 using the substitution of Ce^{3+} ions for Ce atoms. The percentage of Ce^{3+} could change hole-doping concentrations to tune the DOS at E_F . Note that the hole doping of $n_h = 1.0e$ can be enabled by the substitution of 33% Ce^{3+} . In order to examine the electronic miscibility of Ce^{3+} ions in the CeH_9 matrix, we calculate the charge density of CeH_9 without hole doping (see Fig. S7 in the Supplemental Material). Interestingly, we find that the total charge inside the Ce muffin-tin sphere with radius 1.40 \AA is $9.55e$ with including the $5s^25p^6$ semicore electrons, close to that ($9.63e$) obtained at $n_h = 1.0e$. This nearly invariance of Ce charges between the two systems implies that both Ce and Ce^{3+} could behave similarly as cations without hole localization. Based on our results for the charge distribution and structural stability of hole doping $n_h < 1.2e$, Ce^{3+} ions are most likely to be electronically miscible with Ce atoms in the CeH_9 matrix. We note that in the present calculations, the hole charges are compensated by uniform background charge

to maintain charge neutrality, as implemented in the VASP code [39, 40]. This simulation of hole doping is believed to properly describe the incorporated Ce^{3+} ions in the CeH_9 matrix, because both Ce and Ce^{3+} with similar cation characters can be equally screened by their surrounding anionic H cages.

Finally, we also explore the hole-doping effect on SC in a recently observed [22–24] rare earth hydride LaH_{10} . As shown in Fig. 4(a), this hydride has a vHs near E_F with a strong hybridization of La $4f$ and H $1s$ orbitals, similar to the characteristic of vHs in CeH_9 [see Fig. 1(b)]. The calculated λ and T_c values of LaH_{10} are displayed as a function of n_h in Fig. 4(b). Since the DOS around E_F increases with hole doping [see Fig. 4(a)], λ increases monotonously with increasing n_h . Consequently, hole doped LaH_{10} raises T_c from 233 K (without hole doping) to 245 K at $n_h = 0.3e$. Here, the hole doping-induced increase of T_c is 12 K, much smaller than the corresponding $\Delta T_c \approx 62$ K in CeH_9 [see Fig. 3(c)]. The relatively smaller value of ΔT_c in LaH_{10} would be associated with the weak variation of DOS around E_F via hole doping [see Fig. 4(a)].

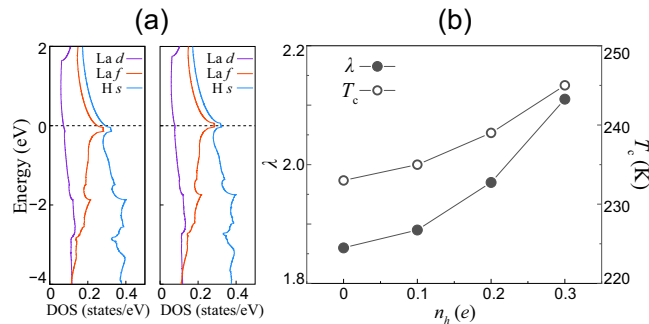


FIG. 4. (a) Partial DOS of LaH_{10} , obtained without hole doping ($n_h = 0$) and at $n_h = 0.1e$. In (b), the calculated λ and T_c values are displayed as a function of n_h .

In summary, based on first-principles calculations, we proposed that hole doping significantly enhances T_c in a recently synthesized [28, 29] hydride CeH_9 . It was revealed that hole doping induces a shift of E_F toward the vHs, thereby leading to the enhancement of EPC through an increased DOS around E_F . Interestingly, the vHs was found to stem from the crossings of two crystalline symmetry-protected DNLs whose electronic states are mostly composed of hybridized Ce $4f$ and H $1s$ orbitals. Therefore, the symmetry, band topology, and hole doping are cooperated to increase T_c of compressed CeH_9 . The proposed hole-doping effect on SC is rather generic and hence, it can also be applicable to another high- T_c rare earth hydride LaH_{10} . We anticipate that future experimental work will be stimulated to adopt hole doping for raising T_c in high-pressure superconducting hydrides.

Acknowledgements. This work was supported by the National Research Foundation of Korea (NRF) grant funded by the Korean Government (Grants No. 2019R1A2C1002975, No. 2016K1A4A3914691, and No. 2015M3D1A1070609).

The calculations were performed by the KISTI Supercomputing Center through the Strategic Support Program (Program No. KSC-2019-CRE-0183) for the supercomputing application research.

C.W. and S.L. contributed equally to this work.

* Corresponding author: chojh@hanyang.ac.kr

-
- [1] H. J. Queisser and E. E. Haller, *Science* **281**, 945 (1998).
 - [2] Y. Tokura, H. Takagi, and S. Uchida, *Nature (London)* **337**, 345 (1989).
 - [3] Y. Cao, V. Fatemi, S. Fang, K. Watanabe, T. Taniguchi, E. Kaxiras, and P. Jarillo-Herrero, *Nature (London)* **556**, 34 (2018).
 - [4] P. A. Lee, N. Nagaosa, and X.-G. Wen, *Rev. Mod. Phys.* **78**, 17 (2006).
 - [5] B. Keimer, S. A. Kivelson, M. R. Norman, S. Uchida, J. Zaanen, *Nature (London)* **518**, 179 (2015).
 - [6] G. R. Stewart, *Rev. Mod. Phys.* **83**, 1589 (2011).
 - [7] P. Dai, *Rev. Mod. Phys.* **87**, 855 (2015).
 - [8] J. G. Bednorz and K. A. Müller, *Z. Phys. B Condens. Matter* **64**, 189 (1986).
 - [9] Y. Kamihara, H. Hiramatsu, M. Hirano, R. Kawamura, H. Yanagi, T. Kamiya, and H. Hosono, *J. Am. Chem. Soc.* **128**, 10012 (2006).
 - [10] Y. Kamihara, T. Watanabe, M. Hirano, and H. Hosono, *J. Am. Chem. Soc.* **130**, 3296 (2008).
 - [11] J. Bardeen, L. N. Cooper, and J. R. Schrieffer, *Phys. Rev.* **106**, 162 (1957).
 - [12] E. Zurek, R. Hoffmann, N. W. Ashcroft, A. R. Oganov, and A. O. Lyakhov, *Proc. Natl. Acad. Sci. USA* **106**, 42 (2009).
 - [13] J. Hooper and E. Zurek, *J. Phys. Chem. C* **116**, 13322 (2012).
 - [14] H. Wang, J. S. Tse, K. Tanaka, T. Litaka, and Y. Ma, *Proc. Natl. Acad. Sci. USA* **109**, 6463 (2012).
 - [15] Y. Xie, Q. Li, A. R. Oganov, and H. Wang, *Acta Cryst. C* **70**, 104 (2014).
 - [16] D. Duan, Y. Liu, F. Tian, D. Li, X. Huang, Z. Zhao, H. Yu, B. Liu, W. Tian, and T. Cui, *Sci. Rep.* **4**, 6968 (2014).
 - [17] X. Feng, J. Zhang, G. Gao, H. Liu, and H. Wang, *RSC Adv.* **5**, 59292 (2015).
 - [18] F. Peng, Y. Sun, C. J. Pickard, R. J. Needs, Q. Wu, and Y. Ma, *Phys. Rev. Lett.* **119**, 107001 (2017).
 - [19] H. Liu, I. I. Naumov, R. Hoffmann, N. W. Ashcroft, and R. J. Hemley, *Proc. Natl. Acad. Sci. USA* **114**, 6990 (2017).
 - [20] Y. Sun, J. Lv, Y. Xie, H. Liu, and Y. Ma, *Phys. Rev. Lett.* **123**, 097001 (2019).
 - [21] H. Xie, Y. Yao, X. Feng, D. Duan, H. Song, Z. Zhang, S. Jiang, S. A. T. Redfern, V. Z. Kresin, C. J. Pickard, and T. Cui, *Phys. Rev. Lett.* **125**, 217001 (2020).
 - [22] A. P. Drozdov, M. I. Erements, I. A. Troyan, V. Ksenofontov, and S. I. Shylin, *Nature (London)* **525**, 73 (2015).
 - [23] M. Somayazulu, M. Ahart, A. K. Mishra, Z. M. Geballe, M. Baldini, Y. Meng, V. V. Struzhkin, and R. J. Hemley, *Phys. Rev. Lett.* **122**, 027001 (2019).
 - [24] A. P. Drozdov, P. P. Kong, V. S. Minkov, S. P. Besedin, M. A. Kuzovnikov, S. Mozaffari, L. Balicas, F. F. Balakirev, D. E. Graf, V. B. Prakapenka, E. Greenberg, D. A. Knyazev, M. Tkacz, and M. I. Erements, *Nature (London)* **569**, 528 (2019).
 - [25] E. Snider, N. Dasenbrock-Gammon, R. McBride, M. Debessai,

- H. Vindana, K. Vencatasamy, K. V. Lawler, A. Salamat, and R. P. Dias, *Nature (London)* **586**, 373 (2020).
- [26] W. A. Bassett, *High Press. Res.* **29**, 163 (2009).
- [27] H. K. Mao, X. J. Chen, Y. Ding, B. Li, and L. Wang, *Rev. Mod. Phys.* **90**, 015007 (2018).
- [28] X. Li, X. Huang, D. Duan, C. J. Pickard, D. Zhou, H. Xie, Q. Zhuang, Y. Huang, Q. Zhou, B. Liu, and T. Cui, *Nat. Commun.* **10**, 3461 (2019).
- [29] N. P. Salke, M. M. Davari Esfahani, Y. Zhang, I. A. Kruglov, J. Zhou, Y. Wang, E. Greenberg, V. B. Prakapenka, J. Liu, A. R. Oganov, and J.-F. Lin, *Nat. Commun.* **10**, 4453 (2019).
- [30] L. Liu, C. Wang, S. Yi, K. W. Kim, J. Kim, and J.-H. Cho, *Phys. Rev. B* **99**, 140501(R) (2019).
- [31] H. Jeon, C. Wang, S. Yi, and J.-H. Cho, *Sci. Rep.* **10**, 16878 (2020).
- [32] D. A. Papaconstantopoulos, M. J. Mehl, and P.-H. Chang, *Phys. Rev. B* **101**, 060506(R) (2020).
- [33] Y. Kim, B. J. Wieder, C. L. Kane, and A. M. Rappe, *Phys. Rev. Lett.* **115**, 036806 (2015).
- [34] C. Fang, Y. Chen, H.-Y. Kee, and L. Fu, *Phys. Rev. B* **92**, 081201(R) (2015).
- [35] G. Bian, T.-R. Chang, R. Sankar, S.-Y. Xu, H. Zheng, T. Neupert, C.-K. Chiu, S.-M. Huang, G. Chang, I. Belopolski, *et al.* *Nat. Commun.* **7** 10556 (2016).
- [36] C. Fang, H. Weng, X. Dai, and Z. Fang, *Chinese Phys. B* **25**, 117106 (2016).
- [37] Q.-F. Liang, J. Zhou, R. Yu, Z. Wang, and H. Weng, *Phys. Rev. B* **93**, 085427 (2016).
- [38] Our DFT calculations were performed using the Vienna *ab initio* simulation package with the projector-augmented wave method [39–41]. For the exchange-correlation energy, we employed the generalized-gradient approximation functional of Perdew-Burke-Ernzerhof (PBE) [42]. The $5s^25p^6$ semicore electrons of Ce atom were included in the electronic-structure calculations. A plane-wave basis was used with a kinetic energy cutoff of 1000 eV. The \mathbf{k} -space integration was done with the $18 \times 18 \times 12$ k points for the structure optimization and the $48 \times 48 \times 32$ k points for the DOS calculation. All atoms were allowed to relax along the calculated forces until all the residual force components were less than 0.001 eV/Å. The lattice dynamics and EPC calculations were carried out by using the QUANTUM ESPRESSO (QE) package [43] with the norm-conserved Hartwigsen-Goedecker-Hutter pseudopotentials [44], a kinetic energy cutoff of 1224 eV, and the $3 \times 3 \times 2$ q and $18 \times 18 \times 12$ k points for the computation of phonon frequencies. For the calculation of EPC, we used the software EPW [45, 46] with the $24 \times 24 \times 16$ q and $48 \times 48 \times 32$ k points.
- [39] G. Kresse and J. Hafner, *Phys. Rev. B* **48**, 13115 (1993).
- [40] G. Kresse and J. Furthmüller, *Comput. Mater. Sci.* **6**, 15 (1996).
- [41] P. E. Blöchl, *Phys. Rev. B* **50**, 17953 (1994).
- [42] J. P. Perdew, K. Burke, and M. Ernzerhof, *Phys. Rev. Lett.* **77**, 3865 (1996); **78**, 1396 (1997).
- [43] P. Giannozzi, S. Baroni, N. Bonini, M. Calandra, R. Car, C. Cavazzoni, D. Ceresoli, G. L. Chiarotti, M. Cococcioni, I. Dabo *et al.*, *J. Phys.: Condens. Matter* **21**, 395502 (2009).
- [44] C. Hartwigsen, S. Goedecker, and J. Hutter, *Phys. Rev. B* **58**, 3641 (1998).
- [45] F. Giustino, M. L. Cohen, and S. G. Louie, *Phys. Rev. B* **76**, 165108(R) (2007).
- [46] S. Poncé, E. R. Margine, C. Verdi, and F. Giustino, *Comput. Phys. Commun.* **209**, 116 (2016).
- [47] The Supplemental Material at <http://link.aps.org/supplemental/xxxxx> for the symmetry and topology analysis, phonon frequencies, band projections onto the orbitals of Ce and H atoms, band structure computed with including SOC, and charge density plot of CeH₉ as well as the DOS of H₃S.
- [48] A. A. Mostofi, J. R. Yates, Y.-S. Lee, I. Souza, D. Vanderbilt, and N. Marzari, *Comput. Phys. Commun.* **178**, 685 (2008).
- [49] Q. S. Wu, S. N. Zhang, H.-F. Song, M. Troyer, and A. A. Soluyanov, *Comput. Phys. Commun.* **224**, 405 (2018).
- [50] N. F.Q. Yuan, H. Isobe, and L. Fu, *Nat. Commun.* **10**, 5769 (2019).
- [51] A. B. Migdal, *Sov. Phys. JETP* **34**, 996 (1958).
- [52] G. M. Eliashberg, *Sov. Phys. JETP* **11**, 696 (1960).
- [53] P. B. Allen and B. Mitrović, *Solid State Phys.* **37**, 1 (1982).